Research Article

For reprint orders, please contact: reprints@futuremedicine.com

Nanomedicine

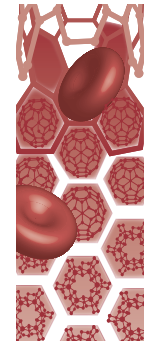

Safe and symptomatic medicinal use of surface-functionalized Mn_3O_4 nanoparticles for hyperbilirubinemia treatment in mice

Nabarun Polley[1], Srimoyee Saha[2], Aniruddha Adhikari[1], Somtirtha Banerjee[2], Soumendra Darbar[3], Sukhen Das[2] & Samir Kumar Pal*[,1]

[1]Department of Chemical, Biological & Macromolecular Sciences, S N Bose National Centre for Basic Sciences, Block JD, Sector III, Salt Lake, Kolkata 700 098, India

[2]Department of Physics, Jadavpur University, 188, Raja Subodh Chandra Mullick Road, Jadavpur, Kolkata 700032, India

[3]Research & Development Division, Dey's Medical Stores (Mfg.) Ltd, 62, Bondel Road, Ballygunge, Kolkata 700019, India

*Author for correspondence: skpal@bose.res.in

Aim: Testing the potential of citrate-capped Mn_3O_4 nanoparticles (NPs) as a therapeutic agent for alternative rapid treatment of hyperbilirubinemia through direct removal of bilirubin (BR) from blood in mice. **Materials & methods:** NPs were synthesized and the mechanism of BR degradation in presence and absence of biological macromolecules were characterized *in vitro*. To test the *in vivo* BR degradation ability of NPs, CCl_4-intoxicated mice were intraperitoneally injected with NPs. **Results:** We demonstrated ultrahigh efficacy of the NPs in symptomatic treatment of hyperbilirubinemia for rapid reduction of BR in mice compared with conventional medicine silymarin without any toxicological implications. **Conclusion:** These findings may pave the way for practical clinical use of the NPs as safe medication of hyperbilirubinemia in human subjects.

Keywords: hyperbilirubinemia • mice model • Mn-based functionalized nanoparticles • nanomedicine • nanotherapy of jaundice

The term hyperbilirubinemia is defined as increased bilirubin (BR) level (>1.3 mg/dl in human) in blood. Hyperbilirubinemia is caused when there is an imbalance between production of BR (resulting from hemolysis, sepsis, blood extravasation or polycythemia) and decrease in BR excretion due to inadequate hepatic conjugation and increased enterohepatic reabsorption (resulting from pyloric stenosis, delayed bacterial gut colonization, GI tract immobility or obstruction) [1–3]. Although at micromolar concentrations BR acts as an antioxidant for scavenging peroxyl radicals in blood [4], yet it can be toxic and harmful to cells at higher concentration [5,6]. Elevated level of BR and its oxidative products in human blood causes various diseases including neonatal jaundice (>10 mg/dl), Gilbert syndrome (with BR level reaching >6 mg/dl), Crigler–Najjar type I disease (>30 mg/dl) [7] and BR-induced neurologic dysfunction [8]. Severe neurotoxicity in case of neonates (Kernicterus) and damage in white matter of adult brain are also the consequences of higher BR level [9,10]. In case of hepatitis E, infection in pregnant women, associated hyperbilirubinemia itself is found to increase the risk of preterm delivery [11]. Treatment options for hyperbilirubinemia include phototherapy [12], hemoperfusion, hemodialysis and exchange blood transfusion [13]. Although phototherapy is widely used and a best choice for the treatment of hyperbilirubinemia in neonates, its efficacy is noted to diminish as children with Crigler–Najjar syndrome advance in age and in particular during adolescence [12,14,15]. Hemoperfusion and exchange blood transfusion have significant morbidity and even mortality [1]. Apart from the mentioned therapeutic procedures various organic, inorganic and phytochemicals have been used for reduction of elevated BR level in blood [16–19]. All these therapeutic drugs function in hepatoprotective way and lack the ability to degrade BR directly [2]. So, none of these became very fruitful in effective and quick reduction of serum BR level. In the above context, a safe, symptomatic and effective therapeutic strat-

Future Medicine part of fsg

egy is extremely needed, and is the principal motive of the present work.

Manganese (Mn), one of the safest materials is a natural constituent, and often a cofactor for enzymes and receptors [20]. In a series of earlier studies from this group, we have established that the charge state of Mn in the citrate-capped Mn_3O_4 nanoparticles (C-Mn_3O_4 nanoparticles [NPs]) is involved in selective catalysis of BR in absence of any photoactivation [21,22]. The mixed valence state of Mn (+2, +3 and +4) along with the functional groups on the surface coordinating ligands of Mn_3O_4 NPs leads to the exceptional catalytic activity. The very fast and selective reduction of the BR level (both conjugated and unconjugated) in the blood specimens in *ex vivo* condition without any significant alteration of other essential blood parameters have also been reported.

In the present study, we have synthesized citrate-capped Mn_3O_4 NPs by ligand-etching technique as described in earlier studies [21,23]. The structural characterization and the interaction with a model-blood protein of the NPs have been performed using high resolution transmission electron microscopy (TEM), steady state and time-resolved optical spectroscopy. Ultrahigh efficacy of generation of reactive oxygen species (ROS) and surface-mediated catalysis of the synthesized NPs, have also been established. We have also performed systematic *in vitro* and *in vivo* preclinical studies on the toxicity of the functionalized NPs. All the measurements confirm that the Mn-based nanomedicine is safe and biocompatible due to lack of any potential toxicity. In order to assess the effectiveness of the NPs as symptomatic nanomedicine in managing hyperbilirubinemia in mice, we have checked the BR concentration and found to become almost normal in 6 h after intraperitoneal injection of the NPs. Therefore, these results demonstrate that the functionalized NPs are strong candidate as effective drug for hyperbilirubinemia treatment, and superior to the commercially available drug, silymarin in terms of efficacy with a satisfactory biocompatibility.

Materials & methods

Materials

Manganese chloride, sodium citrate, NaOH, BR, human serum albumin (HSA), silymarin, heparin, acrylamide, bis-acrylamide, ammonium persulfate, isobutanol, tris base, bromophenol blue, dithiothreitol, tetramethylethylenediamine were obtained from Sigma-Aldrich (MO, USA). 2′, 7′-dichlorofluorescin diacetate (DCFH-DA), Ethanol amine, HCl and glycerol were received from Merck (NJ, USA). All the chemicals used for this study were of analytical grade and were used without further purification.

Synthesis of citrate-functionalized Mn_3O_4 NPs

Synthesis of bulk Mn_3O_4 NPs was done following a reported ultrasonic-assisted approach for preparation of colloidal Mn_3O_4 NPs at normal temperature and pressure without any additional surfactants or templates [23]. For functionalizing the as-prepared Mn_3O_4 NPs by citrate ligand first, 0.5 M citrate (ligand) solution was prepared in Milli-Q (from Millipore) water. Then, the pH of the solutions at approximately seven was adjusted by drop wise addition of 1 (M) NaOH solution. In the ligand solution of pH approximately seven, as-prepared Mn_3O_4 NPs (~100 mg of powder Mn_3O_4 NPs in 5 ml ligand solution) were added and extensively mixed for 12 h in a cyclomixer. Finally, using a syringe filter of 0.22 µm diameter the non-functionalized bigger-sized NPs were filtered out. The resulting filtrated solutions were used for our experiments, both *in vivo* and *in vitro* studies without further dilution [21].

Microscopic & spectroscopic studies

For the characterization of the NPs, TEM samples were prepared by dropping sample stock solutions onto a 300-mesh carbon-coated copper grid and dried overnight in air. Particle sizes were determined from micrographs recorded using an FEI TecnaiTF-20 field-emission high-resolution transmission electron microscope operating at 200 kV. Optical absorbance spectra of the solutions were recorded using a quartz cuvette of 1 cm path length in Shimadzu Model UV-2600 spectrophotometer. For the fluorescence imaging study of liquid NPs, Olympus BX51 fluorescence microscope was used. Jobin Yvon Model Fluoromax-3 Fluorimeter was used to study the characteristic fluorescence excitation and PL spectra of C-Mn_3O_4 NP solutions. Far UV circular dichroism measurements were performed on a JASCO815 spectrometer (from JASCO International Co. Ltd, Tokyo, Japan) by using a 1 cm path-length quartz cell. Fluorescence transients were measured using the 16-channel time-correlated single-photon counting (TCSPC) setup, assembled in the lab with all the components (16-channel PMT module PML-16–1-C, Simple Tau-130EM with SPC-130EM & DCC-100 cards, Express Card 54 and SPCM64 software preinstalled in Lenovo ThinkPad laptop-PC) from Becker & Hickl (Berlin, Germany).

For 283-nm laser excitation, we used a femtosecond coupled TCSPC setup [24]. Briefly, the samples were excited by the third harmonic laser beam (283 nm) of the 850 nm (0.5 nJ per pulse) by using a mode-locked Ti-sapphire laser with an 80 MHz repetition rate (Tsunami, Spectra Physics), pumped by a 10W Millennia (Spectra Physics) followed by a pulse-picker (rate 8 MHz), and a third harmonic generator (Spectra-Phys-

ics, model 3980). The third harmonic beam was used for excitation of the sample inside the TCSPC instrument (instrument response function (IRF = 180 ps) and the second harmonic beam was collected for the start pulse. Fluorescence transients were fitted by a nonlinear least square fitting procedure to a function

$$x(t) = \int_0^t E(t')R(t - t')dt'$$

comprising the convolution of the IRF (E [t]) with a sum of exponentials

$$R(t) = A + \Sigma_{i=1}^{N} B_i e^{\frac{-t}{\tau}}$$

characteristic lifetimes (τ_i), and a background (A). Relative concentration in a multiexponential decay was finally expressed as:

$$Cn = \left(\frac{B_n}{\Sigma_{i=1}^{N} B_i}\right) \times 100$$

The quality of the curve fitting is evaluated by a reduced chi-square and residual data.

Other measurements

In order to investigate the efficacy of the NPs for the generation of ROS, DCFH (dichlorofluorescein) was prepared from DCFH-DA at room temperature by mixing 0.5 ml of 1.0 mM DCFH-DA in methanol with 2.0 ml of 0.01N NaOH [25–27]. The solution was then neutralized with 10 ml of 25 mM NaH_2PO_4, at pH 7.4 and was kept on ice in the dark until use. Native gel electrophoresis studies intend to discriminate between HSA and HSA-NP (after 12 and 24 h of incubation) was performed using native PAGE. The gel was prepared according to standard procedures [11], without the addition of SDS or β-mercaptoethanol. Gradient in the gel was nonlinear. Electrophoresis was conducted in denaturing condition for about 3 h in a vertical apparatus (Aplex 305II) at room temperature, at 120V. After completion, protein bands were stained using Coomassie blue.

Animals

Swiss albino mice of either sex (5–8-weeks old, weighing 28 ± 4 gm) were procured from a Committee for the Purpose of Control and Supervision of Experiments on Animals (CPCSEA) approved animal house (registration number: 50/PO/99/CPCSEA) and housed in standard, clean polypropylene cages in a temperature controlled animal room (temperature 22 ± 3°C; relative humidity 45–60 ± 1%; 12 h light/dark cycle). Water and standard laboratory pellet diet for mice (Hindustan Lever, Kolkata) were available *ad libitum*. All mice were allowed to acclimatize for 1 week prior to experimentation. The animals were maintained according to the guidelines recommended by CPCSEA, New Delhi, India and approved by the Institutional Animal Ethics Committee (Approval number- JU-Dey's/IAEC/09/14, dated 31.01.2014).

Acute toxicity study

Single-dose intraperitoneal toxicity study was conducted to determine the possible acute toxicity of surface-modified Mn_3O_4 NPs following the general principles of the OECD guideline 423 with some adjustments [28]. Twelve female mice were divided in four groups: one control group (received 0.2 ml Milli-Q water) and three experimental groups (received either 600, 2000 or 5000 mg/kg bodyweight (BW) of NP dissolved in 0.2 ml Milli-Q water). All the animals were kept in fasting condition overnight prior to the injection. Behavior, mortality and BW were monitored daily for a period of 14 days.

Treatment protocol: Phase I

Forty eight mice of either sex were randomly divided into six groups of eight mice each. Group I served as the vehicle control and was given olive oil daily (0.5 ml/kg BW) for a period of 2 weeks. Group III served as NP control and left untreated for first 2 weeks, then received citrate-capped Mn_3O_4 NP (500 mg/kg BW dissolved in 0.2ml Milli-Q water) daily for last 7 days. For inducing hyperbilirubinemia and hepatotoxicity (*in vivo*), animals of groups II, IV, V and VI were administered with carbon tetrachloride solution (50% CCl_4 in olive oil) 1 ml/kg BW daily for a period of 2 weeks. CCl_4 is a well-known hepatotoxic agent frequently used to study hepatoprotective activity of new drugs in *in vivo* experimental model. CCl_4 administration induces critical liver damage in mice which in turn simulates a condition of acute hepatitis showing similar symptoms as humans [29–31]. CCl_4 activated by liver enzyme cytochrome P450 forms the trichloromethyl free radical (CCl_3•) that damages hepatic cells [32]. These radicals bind covalently to sulfhydryl groups of glutathione and protein thiols in cells to initiate a chain of events leading to membrane-lipid peroxidation and cell necrosis [33–35]. After CCl_4 intoxication, group III served as the CCl_4 control and was left untreated. Group IV was administered with citrate-capped Mn_3O_4 NP (500 mg/kg BW dissolved in 0.2 ml Milli-Q water) for 7 days. Group V served as citrate control and was treated with citrate (100 µl/mice; 1:1 solution in water). Group VI served as the positive control and was administered silymarin (100 mg/kg BW) [36,37] daily for a period of 1 week. All the treatments were executed by intraperitoneal injection. At the end of the experiment, the animals were

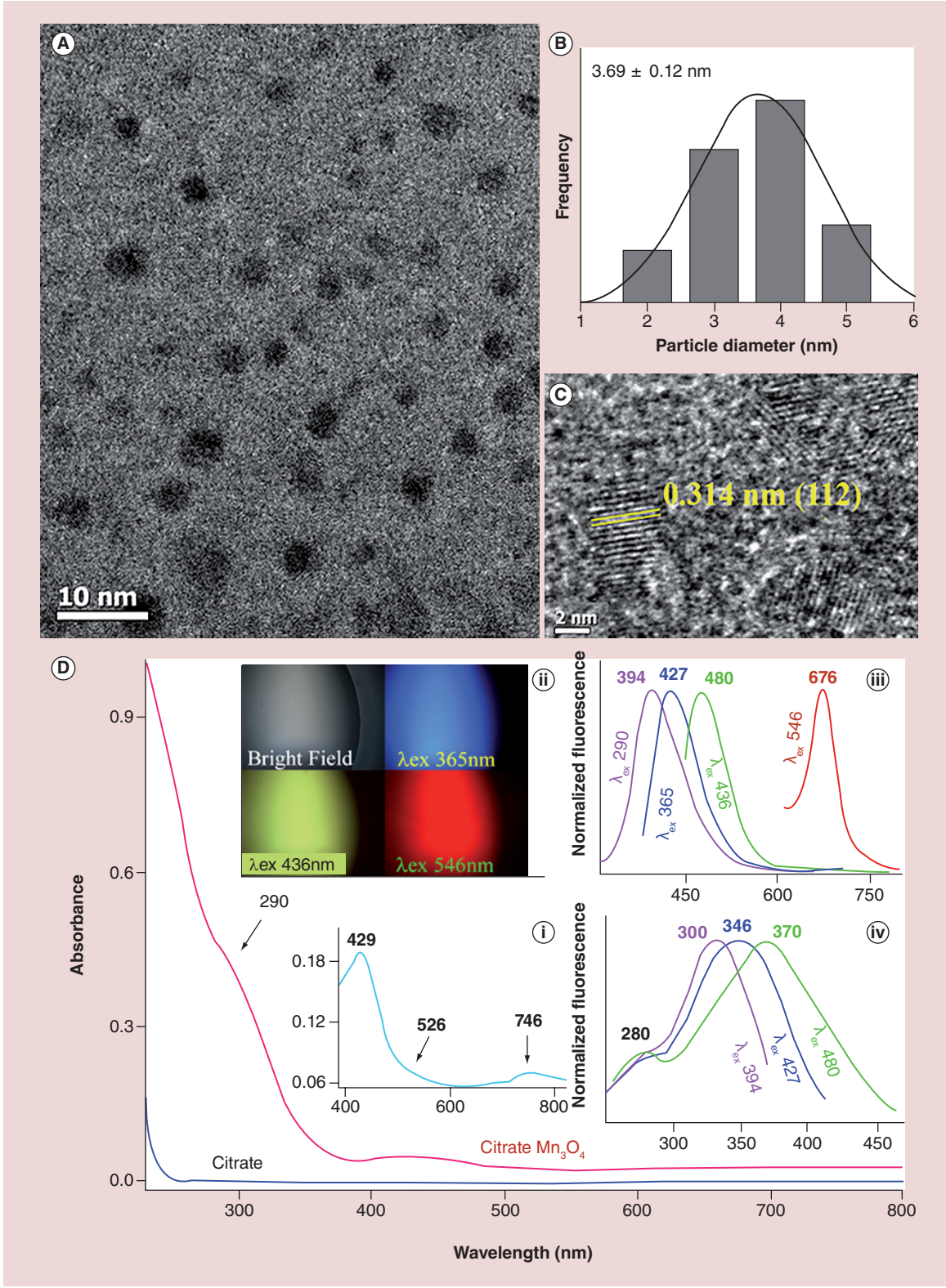

Figure 1. Characterization of nanoparticles. **(A)** The particle distribution of the nanoparticles (NPs) recorded under transmission electron microscopy. **(B)** The particle size distribution is shown with average size of 3.69 ± 0.12 nm and **(C)** high-resolution electron micrograph of the NPs with a clear interplaner distance of 0.314 nm for 112 planes in the Mn_3O_4 NPs is evident.

Figure 1. Characterization of nanoparticles (cont.). **(D)** The absorption spectra of citrate-capped NPs used as nanomedicine in the present study and the capping agent citrate are shown in panel. A magnified version of the absorption spectrum of the NPs in the rage of 400–800 nm is shown in the inset **(i)**. Different absorption peaks due to d-d transitions (see text) are evident. Fluorescence microscopic view of the liquid solution of the NPs with different excitation is shown in the inset **(ii)**. The corresponding emission and excitation spectra of the solution are shown in the insets **(iii& iv)**, respectively.
For color figures, please see online at www.futuremedicine.com/doi/full/10.2217/NNM.15.83

kept in fasting condition overnight and sacrificed by cervical dislocation.

Treatment protocol: Phase II

For studying the efficiency of BR degradation by citrate-capped Mn_3O_4 NP over standard drug silymarin, 48 mice were divided into four groups (n = 12 per group). Group I served as vehicle control and received olive oil daily (0.5 ml/kg BW) for a period of 3 weeks. Other four groups were administered with CCl_4 solution (50% CCl_4 in olive oil) 1 ml/kg BW daily for a period of 3 weeks to induce hyperbilirubinemia. After induction, group II left untreated, group III was administered with citrate-capped Mn_3O_4 NP (500 mg/kg BW dissolved in 0.2 ml Milli-Q water) twice daily and group IV received silymarin (100 mg/kg BW) twice daily. Serum biochemical tests were performed from blood collected at 2, 6, 12 and 24 h.

Measurement of serum biochemical parameters

For biochemical studies, blood samples were collected just before sacrifice in sterile tubes (nonheparinized) from retro-orbital plexus and allowed to clot for 45 min. Serum was separated by centrifugation at 3000 rpm for 15 min. All serum samples were sterile, hemolysis-free, and were kept at 4°C before determination of the biochemical parameters. Serum BR concentration (total and direct) was measured using commercially available test kits and results were expressed as mg/dl. Liver damage was assessed by the estimation of serum activities of alanine aminotransferase (ALT, EC 2.6.1.2), aspartate aminotransferase (AST, EC 2.6.1.1), and alkaline phosphatase (ALP, EC 3.1.3.1), γ-glutamyltranferase (GGT, 2.3.2.2) using commercially available test kits. The results were expressed as units/liter (IU/l). Total protein concentration was estimated and expressed as gm/dL. All the kits for measurement of serum biochemical parameters were purchased from Autospan Liquid Gold, Span Diagnostics Ltd (Surat, India). All hematological tests were performed spectrophotometrically following the protocols described by the corresponding manufacturers.

Hematological study

For hematological studies, the blood was collected in heparinized tubes. Blood-cell count was done using blood smears in Sysmax-K1000 Cell Counter. Parameters studied were hemoglobin, total red blood cell, reticulocyte, hematocrit, mean corpuscular volume, mean corpuscular hemoglobin, mean corpuscular hemoglobin concentration, platelets, total white blood cell.

Histopathological examination

The liver was excised immediately after collection of blood, washed with ice-cold phosphate buffer and dried with tissue paper. It was weighed and fixed in neutral formalin solution (10%), dehydrated in graduated ethanol (50–100%), cleared in xylene and embedded in paraffin. Sections 4–5 µm thick were prepared using microtome and then stained with hematoxylin and eosin (H&E) dye and examined for histopathological changes under the microscope.

Statistical analysis

All quantitative data are expressed as mean ± standard deviation. Comparison of different parameters between the groups was performed using one-way analysis of variance followed by Tukey's multiple comparison test using a computer program GraphPad Prism (version 5.00 for Windows), GraphPad Software, California, USA [38]. $p < 0.05$ was considered significant.

Results & discussion

The spherical Mn_3O_4 NPs were imaged by TEM (Figure 1A) and statistical evaluation found a size distribution of about 3.69 ± 0.12 nm (Figure 1B). Figure 1C is the high resolution TEM image of an isolated Mn_3O_4 NP. The observed interfringe distance of 0.314 nm is consistent with Mn_3O_4 interplanar distance of 112 plane revealing crystalline nature of the NP [21]. The absorbance spectra of the NPs and the capping-ligand citrate are represented in Figure 1D. A magnified view of the absorption spectrum of the NPs in the range of 400–800 nm is shown in the inset Figure 1Di. The absorbance maxima at around 290 and 429 , 526, 746 nm correspond to the high-energy ligand-to-metal charge transfer transition involving citrate–Mn^{4+} interaction and Jahn–Teller (J–T) distorted d–d transitions centered over Mn^{3+} ions respectively [21,22]. The NPs are also found to be fluorescent under various excitation wavelengths as reported earlier [21]. A fluorescence microscopic image containing bright field and fluorescence from the NPs solution under UV (365 nm), blue (436 nm) and green (546 nm) excita-

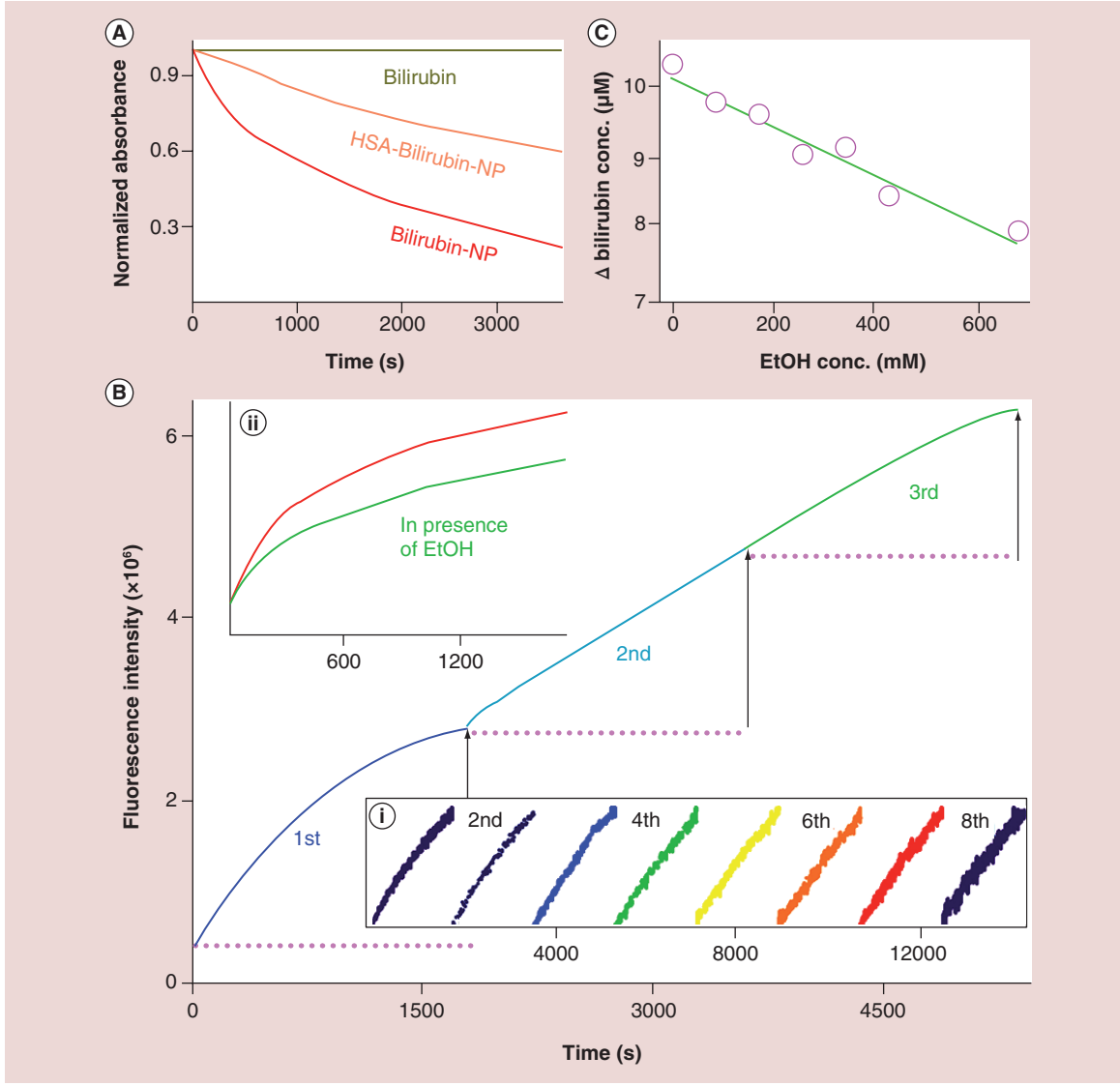

Figure 2. Bilirubin degradation by nanoparticles. Degradation kinetics of bilirubin in solution (*in vitro*) in presence of the nanoparticles (NPs) are shown in **(A)**. Effects of encapsulation of bilirubin in human serum albumin protein and the controlled kinetics of bilirubin in absence of NPs in our experimental condition are also shown in the panel. The efficacy of generation of reactive oxygen species, the key for the degradation of bilirubin for a number of cycles are shown in **(B)**. Reusability of the NPs (inset **[i]**) over eight cycles and reduction of the efficacy in presence of reactive oxygen species quencher ethanol (inset **[ii]**) are also shown. A linear dependency concentration of bilirubin degradation in 1 h on the concentration of ethanol is shown in **(C)**.
conc.: Concentration.

tion is shown in the inset Figure 1Dii. The corresponding emission spectra of the NPs solution are shown in Figure 1Diii, revealing distinct emission peaks for different excitation wavelengths. Different peaks in the excitation spectra (Figure 1Div) form the solution for different detection wavelengths, confirm the multiple excited state in the emission from the NPs as detailed in earlier literature [21].

In order to investigate the efficacy of the NPs in BR degradation *in vitro*, we have monitored BR decomposition at pH = 7.4 in presence and absence of the serum protein HSA (Figure 2A). We have maintained the concentration of the NPs similar to that used in the *in vivo* experiment (from same stock solution). The characteristic absorbance of BR at 450 nm has been chosen for monitoring the kinetic study using UV-visible spectroscopy. Figure 2A shows the relative concentration (C_t/C_0) of BR plotted against reaction time. In absence of HSA, decomposition of BR after 60 min by the NPs can be observed to be around 80%, whereas in presence of HSA, the decomposition reduced to 40%. In contrast to the catalytic decomposition of BR,

only 2–5% of BR degradation is observed without the NPs. These results are self-explanatory, since the water soluble BR gets either higher chance to interact with NPs than in the albumin protein or more accessible to the NPs-generated radical in the aqueous solution [21]. Here, we have found that the NPs are efficient generator of ROS in aqueous solution. Enhanced emission of an ROS indicator DCFH is used for the monitoring of oxidative stress in the solution. The emission maxima of DCFH (520 nm) upon excitation at λ_{ex}=488 nm was plotted against time to generate the fluorescence kinetic plot (Figure 2B) for repetitive addition of DCFH in the solution. The NPs were capable of producing ROS for at least eight cycles as highlighted in Figure 2Bi. The reduction in oxidative stress generation has also been observed in presence of well-known ROS quencher ethanol [21] in the medium (Figure 2Bii). Figure 2C clearly indicates that the generated ROS was inefficient to degrade the BR with increased level of ethanol concentration.

The observed reduction efficacy of the NPs in presence of HSA (Figure 2A) could be rationalized in the following two ways. First, the BR may interact directly with the NPs and undergoes surface-mediated catalysis (Langmuir-Hinshelwood type) and encapsulation of the BR in the presence of HSA hinders the interaction leading to less degradation of BR. Second, the NPs could be encapsulated by the protein HSA for the less interaction with the BR in the aqueous solution. We have ruled out the first possibility by an attempt to study the rate of BR degradation kinetics with the concentration of the NPs in the solution. The rate of the kinetics was found to be independent of the NPs concentration, which should not be the case of surface-mediated catalysis. In order to address the second possibility, we have investigated the interaction of the NPs with the protein HSA as shown in Figure 3. The far-UV circular dichroism spectra of HSA, exhibited two negative bands in the UV region at 208 and 220 nm (Figure 3A), characteristic of an α-helical structure of protein [39]. The percentage of helix content of HSA both in presence and absence of NPs is found to be similar revealing insignificant conformational alteration in α-helical structure of HSA in presence of the NPs. The molecular mass of the protein HSA in presence of the NPs is also found to be intact as shown in native gel electrophoresis study (Figure 3B). A direct evidence of the nature of interaction of the NPs with the protein is clear from picosecond resolved fluorescence transient of the single tryptophan Trp-214 (excitation 283 nm) in absence and presence of the NPs as shown in Figure 3C (average lifetime of 1.95 ns). In case of proximity of the NPs to Trp-214, a quenching of the fluorescence is unavoidable due to Förster

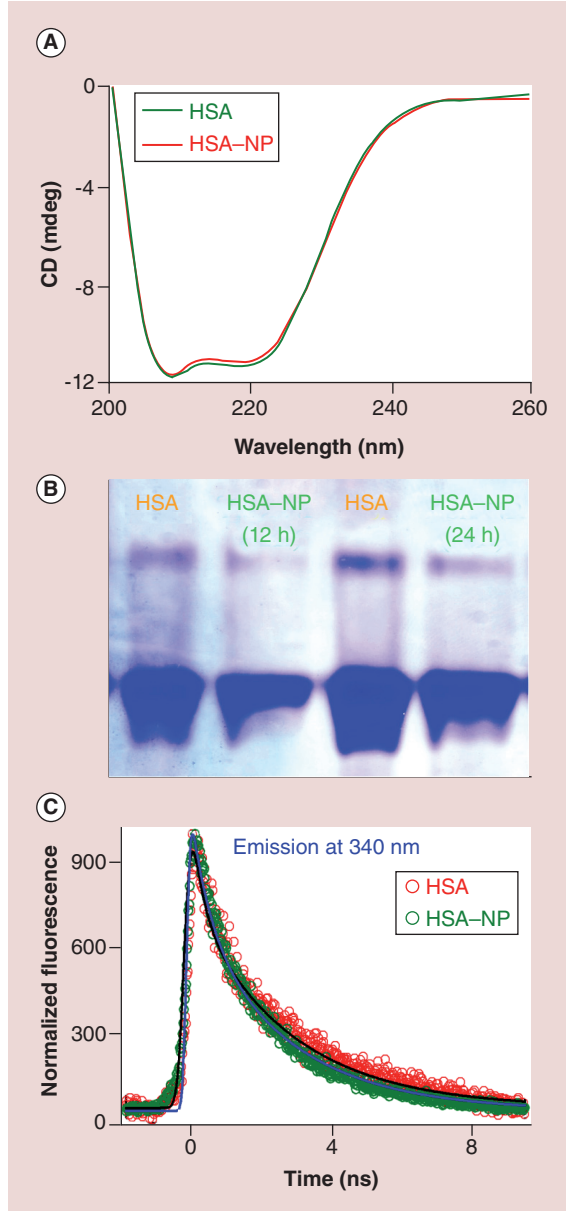

Figure 3. Human serum albumin–nanoparticle interaction. (A) Circular dichroism spectra of HSA without and with the NPs (see text). An insignificant effect of the NPs in the secondary structure of the serum protein is evident. **(B)** The overall structural integrity of the protein upon interaction with the NPs with various incubation time is shown from the mobility of the protein in a native gel. **(C)** Picosecond resolved transient of the single tryptophan (Trp-214) of the serum protein without and with the NPs. In case of direct interaction of the NPs with the protein, quenching (due to Förster resonance energy transfer) of the transient in presence of the NPs is unavoidable because of the strong spectral overlap of the tryptophan emission and absorption of the NPs. However, insignificant quenching of Trp-214 in presence of NPs rules out the possibility of direct interaction (see text).
HSA: Human serum albumin; NP: Nanoparticle.

resonance energy transfer (FRET) [40] as a result of strong spectral overlap of the Trp-214 emission with the absorption of the NPs (Figure 1D). Insignificant change in the Trp-214 emission transient in presence of the NPs, clearly rules out proximal interaction of the protein with the NPs.

For assessing the maximal-tolerated dose of surface-functionalized Mn_3O_4 NP, we performed single-dose acute toxicity study as per OECD guideline. Intraperitoneal injection of Mn_3O_4 NP did not cause any mortality throughout the experimental period for all three dose groups. Behavioral and physical symptoms of acute toxicity such as decreased activity or decreased uptake of food and water were not also been observed during the study period. As no clinical signs of toxicity were observed upto 5000 mg/kg BW, hence 1/10th of the maximum dose administered (i.e., 500 mg/kg BW) was selected for the present study.

In the phase I study, the total serum BR (Tsb) level of CCl_4 treated group (group II) increased to 0.89 ± 0.07 mg/dl which is far higher than the control group (group I; 0.32 ± 0.04 mg/dl), indicative of hyperbilirubinemia. This group (group II) was left untreated for a week to see the auto recovery. The serum biochemical tests were done after treatment of seven days and represented in Table 1. The results show that treatment with the NPs significantly decreased BR level (total and direct) even lower than the sham control (Figure 4A & B). But for group II, we have seen very mild decrease in serum BR concentration even after removal of the hepatoxin, indicating slow recovery process. However, in case of direct BR level, the reduction is not significantly different from the clinical standard silymarin (Table 1). The NPs directly interacts with the BR and degrade the same. In the case of direct BR (soluble in aqueous environments and complex with glucuronic acid), hindrance of the interaction with NPs could be a possible reason of lower efficacy of the NP in reducing direct BR.

For assessing the efficiency of BR degradation *in vivo* by NPs over standard drug silymarin, we performed the second phase of experiment. Here, BR concentration was monitored for a period of 24 h after intoxication. Three weeks CCl_4 intoxication increased the total serum BR level upto 1.28 ± 0.14 mg/dl. Single dose of Mn_3O_4 NP decreases Tsb to 0.40 ± 0.07 mg/dl within 2 h and back to normal level (0.32 ± 0.05 mg/dl) within 6 h compared with the silymarin treated group 1.22 ± 0.16 mg/dl (2 h) and 1.10 ± 0.14 mg/dl (6 h), respectively. The results are represented in Figure 4C & D. Treatment with NPs decreased Tsb level almost 70% compared with that of silymarin (8%) in 2 h and restored normal Tsb concentration within 6 h. The results suggest the efficiency of citrate-functionalized Mn_3O_4 NP in targeted degradation of BR in a much faster rate compared with that of standard drug silymarin in *in vivo* experimental system.

For assessment of liver injury, serum activity of various hepatic lysosomal enzymes is used as diagnostic indicators [41]. Earlier studies have shown that CCl_4 administration increases serum levels of AST, ALT, ALP and GGT [16–19,42–45]. Normal liver contains high concentrations of these enzymes. When there is hepatocyte necrosis or membrane damage, these enzymes are released into the circulation, as indicated by elevated serum enzyme levels [46]. The hepatotoxicity of CCl_4 was confirmed in our study by a significant elevation of serum ALT (197.86%), AST (157.63%), ALP (106.77%) and GGT (105.36%) activities in the CCl_4-treated group as compared with the vehicle control which are summarized in Table 2. However, treatment with NPs at a dose of 500 mg/kg BW for 7 days

Table 1. Effect of nanoparticles on serum bilirubin level in CCl_4-intoxicated mice.

Group	Design of treatment	Total bilirubin (mg/dl)		Direct bilirubin (mg/dl)	
		After induction	After treatment	After induction	After treatment
I	Sham control	0.33 ± 0.05	0.32 ± 0.04†	0.19 ± 0.008	0.20 ± 0.009†,§
II	CCl_4 control	0.89 ± 0.07	0.58 ± 0.04‡,§	0.39 ± 0.054	0.33 ± 0.044‡,§
III	NP control	0.34 ± 0.04	0.18 ± 0.04†,‡,§	0.21 ± 0.009	0.11 ± 0.019†,‡
IV	CCl_4 + NPs	0.93 ± 0.06	0.19 ± 0.03†,‡,§	0.42 ± 0.045	0.13 ± 0.019†,‡
V	CCl_4 + citrate	0.88 ± 0.06	0.52 ± 0.05‡,§	0.38 ± 0.036	0.32 ± 0.034‡,§
VI	CCl_4 + silymarin	0.87 ± 0.07	0.33 ± 0.04†	0.38 ± 0.038	0.13 ± 0.019†,‡

Data are expressed as mean ± standard deviation (n = 8).
One-way analysis of variance Tukey *post hoc*:
$^{\dagger}p < 0.05$ compared with CCl_4.
$^{\ddagger}p < 0.05$ compared with vehicle control.
$^{\S}p < 0.05$ compared with silymarin.
Dosage: Olive oil: 0.5 ml/kg bodyweight; CCl_4 + olive oil sol.: 1 ml/kg bodyweight; NPs: 500 mg/kg bodyweight; silymarin: 100 mg/kg bodyweight; Citrate (1:1 solution in water): 100 µl/mice.
NP: Nanoparticle.

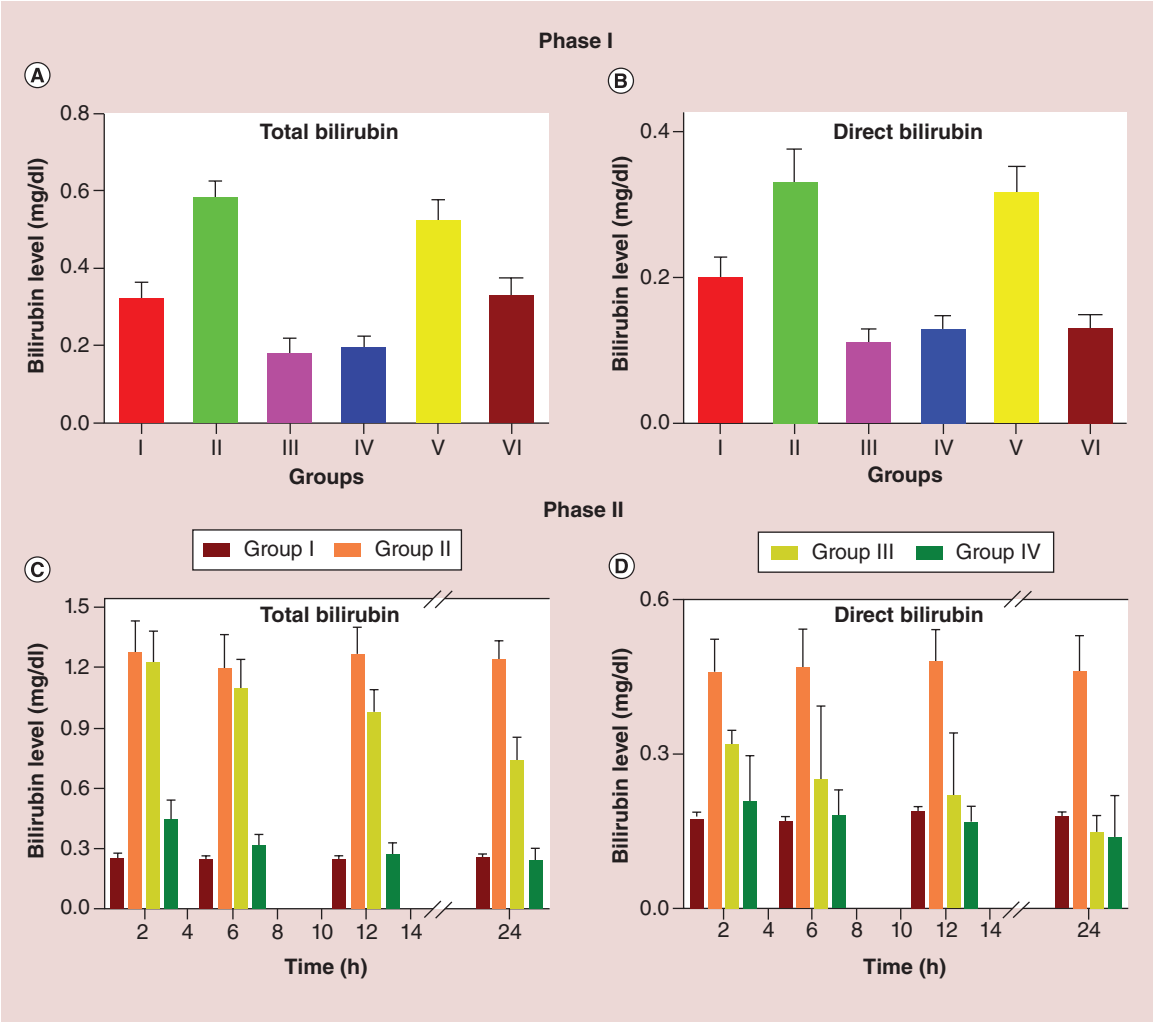

Figure 4. Effect of nanoparticles on bilirubin level *in vivo*. Assay results of total and direct bilirubin concentration in the blood specimens of mice in Phase I **(A & B)** and Phase II **(C & D)**. In Phase II study, single dose of nanoparticles was able to restore normal serum bilirubin level in less than 6 h from hyperbilirubinemia condition. Data are plotted as mean ± standard error of the mean.

decreased the percentages of AST, ALP and GGT by 53.93, 13.01 and 10.82%, respectively, compared with the CCl_4-treated group. The liver function parameters for the NP control group (group III) remain almost same as the vehicle control group indicating no toxicity of the NPs on liver. Furthermore, no significant change in serum protein concentration indicates the nontoxic effect of NP which is in agreement with the *in vitro* study involving HSA, described in the earlier section. The statistical analysis of the all liver biochemical-parameters (except BR) is represented in Table 2. The hematological status of animals of group I, group II, group III and group IV has been assessed and are given in the Table 3. It is evident that there is insignificant change in the hematological parameters across the four groups. The result clearly shows that the presence of NPs does not affect hematological system.

The histopathological observations also support the results obtained from serum biochemical assays (Figure 5). The liver lobules of the vehicle control animals (group I) showed a classical structure with hepatocyte plates directed from the portal triads toward the central vein, where they freely anastomose. The liver sinusoids are normally irregularly dilated and spaces of Disse can be seen. The liver sections of this group showed normal hepatic cells, that is, with well-preserved cytoplasm and prominent nucleus, nucleolus (Figure 5i). The livers of CCl_4-intoxicated mice (group II, Figure 5ii) revealed moderate to severe hepatocellular vacuolization, hepatic necrosis and swelling, bile-duct hyperplasia and increasing cellular mitosis as well as dilation of Disse spaces with focal disruption of the sinusoidal endothelium, inflammatory infiltrations of the portal triads (Figure 5ii) and distortion of the central venules. Mononuclear cell infiltration, hemor-

Table 2. Effect of nanoparticles on ALT, AST, ALP, GGT and total protein in CCl_4-intoxicated mice.

Group	Design of treatment	AST (IU/l)	ALT (IU/l)	ALP (IU/l)	GGT (IU/l)	Total protein (gm/dl)
I	Sham control	81.43 ± 7.31†	19.67 ± 1.67‡,§	26.30 ± 2.63†	2.61 ± 0.30‡,§	6.28 ± 0.54
II	CCl_4 control	209.78 ± 22.77‡,§	58.58 ± 3.28‡,§	54.38 ± 5.48‡,§	5.36 ± 0.66‡	5.78 ± 0.40
III	NP control	79.45 ± 8.32†	17.95 ± 1.92‡,§	24.58 ± 3.14†	2.60 ± 0.42‡,§	6.12 ± 0.64
IV	CCl_4 + NPs	96.65 ± 7.72†	59.58 ± 3.81‡,§	47.30 ± 5.88†,‡	4.78 ± 0.53‡	5.88 ± 0.44
V	CCl_4 + citrate	66.98 ± 10.19†	42.72 ± 3.28†,‡,§	40.23 ± 4.41†,‡	4.78 ± 0.48‡	5.78 ± 0.44
VI	CCl_4 + silymarin	86.43 ± 9.44†	26.79 ± 2.89†,‡	45.98 ± 4.69†,‡	4.61 ± 0.47†,‡	5.78 ± 0.42

Data are expressed as mean ± standard deviation (n = 8).
One-way analysis of variance Tukey *post hoc*:
$^{\dagger}p < 0.05$ compared with CCl4.CCl_4.
$^{\ddagger}p < 0.05$ compared with vehicle control.
$^{\S}p < 0.05$ compared with silymarin.
Dosage:- Olive oil: 0.5 ml/kg bodyweight; CCl_4 + olive oil sol.: 1 ml/kg bodyweight; NPs: 500 mg/kg bodyweight; silymarin: 100 mg/kg bodyweight; citrate (1:1 solution in water): 100 µl/mice.
ALP: Alkaline phosphatase; ALT: Alanine aminotransferase; AST: Aspartate aminotransferase; GGT: γ-glutamyltranferase; NP: Nanoparticle.

rhage, fatty degeneration and formation of regenerative nodules were also observed in CCl_4-treated group indicating that CCl_4 induced severe damage to the hepatic cells. The animals treated with NPs (group IV) and silymarin (group VI) (Figure 5iv & vi, respectively) revealed slight to mild hepatocellular vacuolation and better preservation of the normal liver architecture, with moderate hepatocyte plate disorganizations and smaller dilations of Disse spaces. These treated animals displayed rare periportal inflammatory infiltrate in the liver lobules. The animals treated with only NPs (group III) showed normal liver architecture comparable with the vehicle control group. This indicates the nontoxic effect of citrate-capped Mn_3O_4 on hepatocytes which are in good correlation with the liver function tests. It has been reported that CCl_4 causes necrosis, [42,47–50] fibrosis, [47,51–53] mononuclear cell infiltration, [49,53] steatosis and foamy degeneration of hepatocytes, increase in mitotic activity [54] and cirrhosis [42,49] in liver. Therefore, our histopathological findings in the liver due to CCl_4 administration are in agreement with previous studies. However, treatment with NPs significantly decreased these hepatotoxicity characteristics in mouse liver, suggesting that NPs provided protection against CCl_4-induced liver injury. So, according to the microscopic examinations, severe liver damage induced by CCl_4 was remarkably reduced by the administration of the NPs, which was in good correlation with the results of the liver-functional parameters of the serum.

Conclusion

We have synthesized the NPs with the ultrahigh efficacy toward degradation of BR by a simple and green solution-based technique. We further demonstrated

Table 3. Hematological parameters as studied across the group I (sham control), group II (CCl_4 control), group III (nanoparticle control), group IV (CCl_4 + nanoparticle).

Hematological parameters	Groups			
	I	II	III	IV
Hb (gm/dl)	13.57 ± 1.04	13.95 ± 0.89	13.84 ± 0.92	13.90 ± 0.85
RBC (×10^6/µl)	6.48 ± 0.56	6.40 ± 0.52	6.45 ± 0.48	6.50 ± 0.58
Rt (%)	1.25 ± 0.19	1.18 ± 0.21	1.22 ± 0.32	1.22 ± 0.23
HCT (%)	40.50 ± 3.42	41.12 ± 3.09	39.85 ± 3.16	40.63 ± 2.13
MCV (fl)	62.72 ± 6.06	64.67 ± 7.81	62.42 ± 5.54	63.02 ± 7.32
MCH (pg)	21.02 ± 2.05	21.94 ± 2.46	21.36 ± 2.48	21.52 ± 2.21
MCHC (gm/dl)	40.50 ± 0.61	33.96 ± 0.85	38.54 ± 3.12	34.23 ± 1.68
Platelets (×10^3/µl)	6.53 ± 0.56	6.50 ± 0.55	6.55 ± 0.61	6.42 ± 0.58
WBC (×10^5/µl)	6.38 ± 0.58	6.65 ± 1.05	6.36 ± 0.95	6.78 ± 0.85

Data are expressed as mean ± standard deviation (n = 8).
Hb: Hemoglobin; HCT: Hematocrit; MCH: Mean corpuscular hemoglobin; MCHC: Mean corpuscular hemoglobin concentration; MCV: Mean corpuscular volume; RBC: Red blood corpuscle; Rt: Reticulocyte; WBC: White blood corpuscle.

that these Mn-based NPs are safe, biocompatible and effective-targeted probes for hyperbilirubinemia in mice model based on the *in vitro* and *in vivo* assessments, especially without any toxicological implications. The study to compare the efficacy of the NPs with that of a commercially available drug silymarin shows that in hyperbilirubinemia mice, administration of the NPs brings the BR level to normal limits in 6 h whereas silymarin needs several days to control hyperbilirubinemia in mice. The overall therapeutic procedure is pictorially presented in Figure 6. These findings break through the bottleneck in therapeutic procedures for the treatment of hyperbilirubinemia by fast and direct degradation of BR and pave the way for the practical clinical therapy of Mn-based NPs as safe nanomedicines.

Future perspective

In the years to come, advances in engineering nanomaterials with exquisite size and shape control will expand their use in biomedical applications and open the door of personalized medicine. Our study has shown the potential use of Mn-based NPs directly as therapeutic agent against hyperbilirubinemia. The targeted *in vivo* BR degradation ability of surface-functionalized

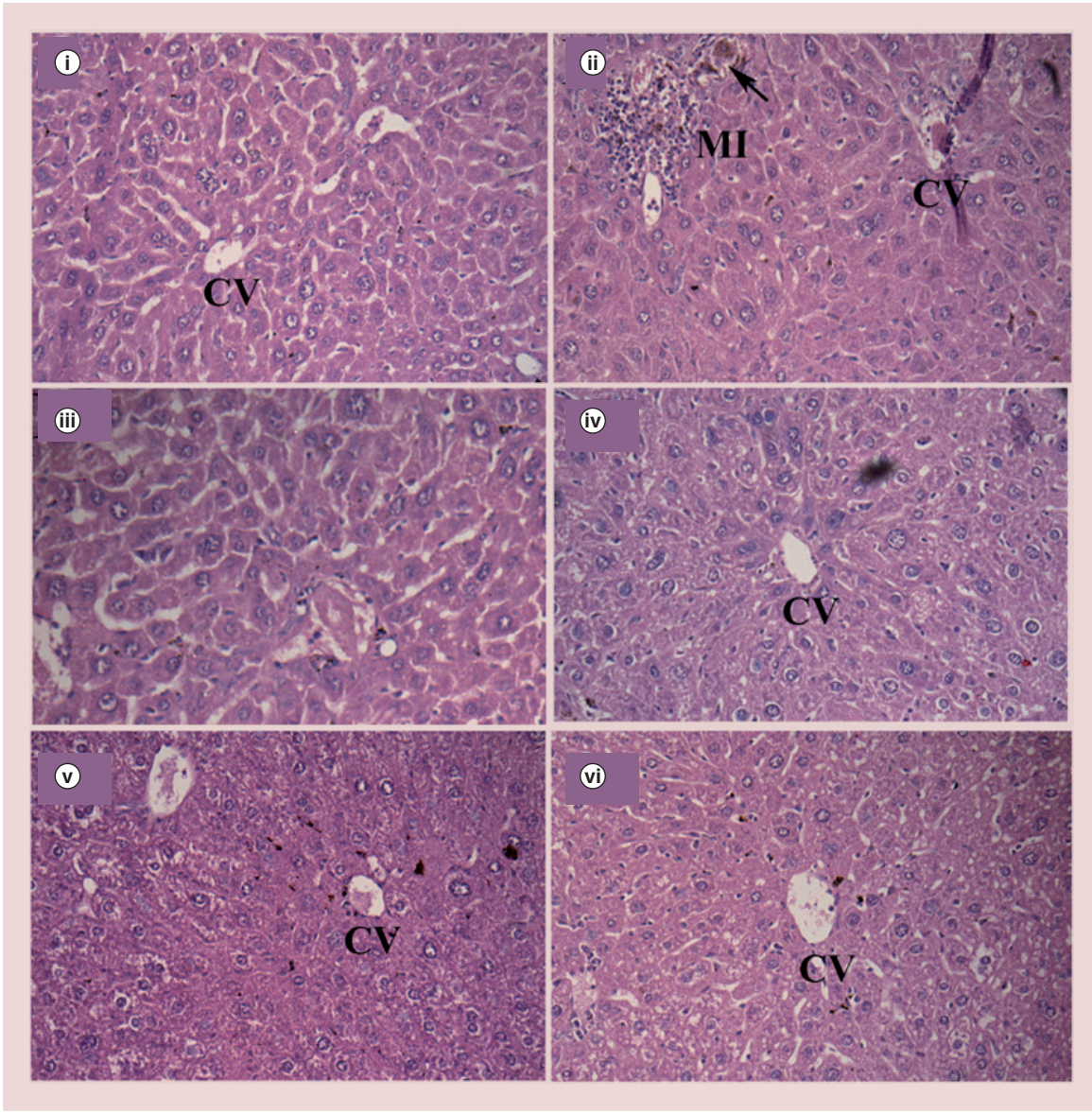

Figure 5. Effect of nanoparticles on hepatic morphological analysis in CCl_4-intoxicated mice. Livers were sectioned and stained with hematoxylin eosin by standard techniques (taken under 100× magnification). Arrows indicate hemorrhage. **(I)** Sham control, **(II)** CCl_4 control, **(III)** nanoparticle control, **(IV)** nanoparticle treated, **(V)** citrate control and **(VI)** Silymarin.
CV: Central vein; MI: Mononuclear cell Infiltration.

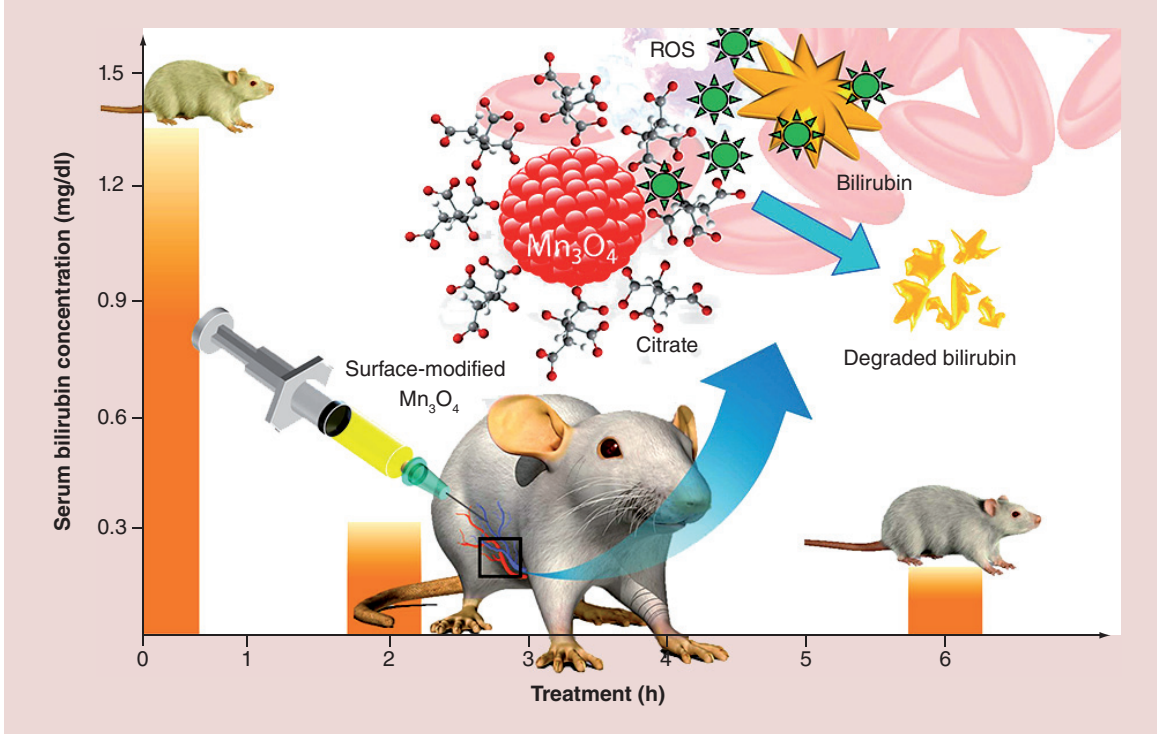

Figure 6. Schematic representation of the nanotherapy using surface-modified Mn_3O_4 nanoparticles. The efficacy of the nanoparticles in reducing serum bilirubin in mice in hours without any side-effect is also represented (see text).
ROS: Reactive oxygen species.

Mn_3O_4 NPs may elucidate a new approach in the symptomatic treatment of hyperbilirubinemia and associated disorders compared with the use of conventional hepatoprotective drugs. A detailed toxicological assessment, pharmacokinetic study and experimentation on more robust genetically modified animal models of hyper-

Executive summary

Background
- Hyperbilirubinemia is one of the most common diseases in tropical countries causing several neurologic damages for neonates as well as adults and if untreated may lead to morbidity and even mortality.
- Current therapeutics for hyperbilirubinemia are poorly effective, nontargeted and time consuming. Also there is no medicine available which can degrade bilirubin directly in *in vivo* condition.

Outcomes of the study
- In this study, the authors demonstrate that intraperitoneally injected citrate-functionalized Mn_3O_4 nanoparticles (NPs) degrade bilirubin very fast and in a specific, nontoxic way compared with conventional drugs in a mouse model.

Methods
- Synthesis and characterization of citrate-functionalized Mn_3O_4 NPs have been done.
- The *in vitro* catalytic activity of NPs in degradation of bilirubin through reactive oxygen species mechanism has been established.
- *In vivo* preclinical studies of Mn_3O_4 NPs as a therapeutic agent against hyperbilirubinemia were done using mice as a model organism.
- The efficiency of Mn_3O_4 NPs in treatment of hyperbilirubinemia in mice is ensured by biochemical tests and histopathological studies.

Conclusion & future perspective
- Our results confirmed that Mn-based NPs are nontoxic, biocompatible and effective targeted probes against hyperbilirubinemia.
- This study may open a new door for faster, safer and efficient therapeutic treatment of hyperbilirubinemia, jaundice and associated diseases.
- This approach may be applied for future nanomedicine applications.

bilirubinemia (e.g., UGT1 A1 deficient mice or Gunn rat model of neonatal jaundice) will help to verify the potential of this nanoparticle in preclinical studies more strongly and lead the way to clinical trials. Finally, it is concluded, in view of good safety margin and faster action with the proposed nanomedicine (NPs), that the medicine could become the symptomatic treatment of choice in hyperbilirubinemia in general.

Acknowledgements

The authors would like to thank Anupam Giri, PRF, DMSE, Yonsei University, South Korea for his help in nanoparticle synthesis.

Financial & competing interests disclosure

N Polley thanks DST, India for Inspire Research Fellowship. The authors thank DAE (India) for financial grant, 2013/37P/73/BRNS and ICMR for financial support (2014-2751). The authors also thank DST, India for financial grants, DST/TM/SERI/2k11/103 and SB/S1/PC-011/2013. The authors have no other relevant affiliations or financial involvement with any organization or entity with a financial interest in or financial conflict with the subject matter or materials discussed in the manuscript apart from those disclosed.

No writing assistance was utilized in the production of this manuscript.

Ethical conduct of research

The authors state that they have obtained appropriate institutional review board approval or have followed the principles outlined in the Declaration of Helsinki for all human or animal experimental investigations. In addition, for investigations involving human subjects, informed consent has been obtained from the participants involved.

References

Papers of special note have been highlighted as:
• of interest; •• of considerable interest

1 Burgos AE, Flaherman VJ, Newman TB. Screening and follow-up for neonatal hyperbilirubinemia a review. *Clin. Pediatr.* 51(1), 7–16 (2012).

• **State-of-the-art review of current therapeutic strategies used in the treatment of hyperbilirubinemia.**

2 Dennery PA, Seidman DS, Stevenson DK. Neonatal hyperbilirubinemia. *N. Engl. J. Med.* 344(8), 581–590 (2001).

•• **Important review regarding hyperbilirubinemia; cause, danger and treatment.**

3 Alkhotani A, Eldin EEMN, Zaghloul A, Mujahid S. Evaluation of neonatal jaundice in the Makkah region. *Sci. Rep.* 4, 4802 (2014).

4 Maghzal GJ, Leck M-C, Collinson E, Li C, Stocker R. Limited role for the bilirubin-biliverdin redox amplification cycle in the cellular antioxidant protection by biliverdin reductase. *J. Biol. Chem.* 284(43), 29251–29259 (2009).

5 Mireles LC, Lum MA, Dennery PA. Antioxidant and cytotoxic effects of bilirubin on neonatal erythrocytes. *Pediatr. Res.* 45(3), 355–362 (1999).

6 Kapitulnik J. Bilirubin: an endogenous product of heme degradation with both cytotoxic and cytoprotective properties. *Mol. Pharmacol.* 66(4), 773–779 (2004).

7 Mahtab MA. *Liver: A Complete Book on Hepato-Pancreato-Biliary Diseases.* Elsevier Health Sciences APAC, Gurgaon, India (2012).

8 Shapiro SM. Chronic bilirubin encephalopathy: diagnosis and outcome. *Semin. Fetal. Neonatal. Med.* 15(3), 157–163 (2010).

9 Lakovic K, Ai J, D'abbondanza J *et al.* Bilirubin and its oxidation products damage brain white matter. *J. Cereb. Blood Flow Metab.* 34(11), 1837–1847 (2014).

10 Hyperbilirubinemia ASON. Neonatal jaundice and kernicterus. *Pediatrics* 108(3), 763–765 (2001).

11 Shalan MG, Mostafa MS, Hassouna MM. El-Nabi SEH, El-Refaie A. Amelioration of lead toxicity on rat liver with vitamin C and silymarin supplements. *Toxicology* 206(1), 1–15 (2005).

12 Van Der Veere CN, Sinaasappel M, Mcdonagh AF *et al.* Current therapy for Crigler–Najjar syndrome type 1: report of a world registry. *Hepatology* 24(2), 311–315 (1996).

13 Xia B, Zhang G, Zhang F. Bilirubin removal by Cibacron Blue F3GA attached nylon-based hydrophilic affinity membrane. *J. Membr. Sci.* 226(1–2), 9–20 (2003).

14 Toietta G, Mane VP, Norona WS *et al.* Lifelong elimination of hyperbilirubinemia in the Gunn rat with a single injection of helper-dependent adenoviral vector. *Proc. Natl Acad. Sci. USA* 102(11), 3930–3935 (2005).

15 Strauss K, Robinson D, Vreman H, Puffenberger E, Hart G, Morton DH. Management of hyperbilirubinemia and prevention of kernicterus in 20 patients with Crigler–Najjar disease. *Eur. J. Pediatr.* 165(5), 306–319 (2006).

16 Kus I, Colakoglu N, Pekmez H, Seckin D, Ogeturk M, Sarsilmaz M. Protective effects of caffeic acid phenethyl ester (CAPE) on carbon tetrachloride-induced hepatotoxicity in rats. *Acta Histochem.* 106(4), 289–297 (2004).

17 Kus I, Ogeturk M, Oner H, Sahin S, Yekeler H, Sarsilmaz M. Protective effects of melatonin against carbon tetrachloride-induced hepatotoxicity in rats: a light microscopic and biochemical study. *Cell Biochem. Funct.* 23(3), 169–174 (2005).

18 Mansour MA. Protective effects of thymoquinone and desferrioxamine against hepatotoxicity of carbon tetrachloride in mice. *Life Sci.* 66(26), 2583–2591 (2000).

19 Babalola OO, Anetor JI, Adeniyi FA. Amelioration of carbon tetrachloride-induced hepatotoxicity by terpenoid extract from leaves of vernonia amydgalina. *Afr. J. Med. Sci.* 30(1–2), 91–93 (2001).

20 Pan D, Caruthers SD, Hu G *et al.* Ligand-directed nanobialys as theranostic agent for drug delivery and manganese-based magnetic resonance imaging of vascular targets. *J. Am. Chem. Soc.* 130(29), 9186–9187 (2008).

21 Giri A, Goswami N, Sasmal C *et al.* Unprecedented catalytic activity of Mn_3O_4 nanoparticles: potential lead of a sustainable therapeutic agent for hyperbilirubinemia. *R. Soc. Chem. Adv.* 4(10), 5075–5079 (2014).

•• ***Ex vivo* study reporting bilirubin-degrading activity of Mn_3O_4 nanoparticles.**

22 Giri A, Goswami N, Pal M *et al.* Rational surface modification of Mn_3O_4 nanoparticles to induce multiple photoluminescence and room temperature ferromagnetism. *J. Mater. Chem. C* 1(9), 1885–1895 (2013).

23 Lei S, Tang K, Fang Z, Zheng H. Ultrasonic-assisted synthesis of colloidal Mn_3O_4 nanoparticles at normal temperature and pressure. *Cryst. Growth. Des.* 6(8), 1757–1760 (2006).

• **Described the synthesis procedure of Mn_3O_4 nanoparticle used.**

24 Saha R, Rakshit S, Pal SK. Molecular recognition of a model globular protein apomyoglobin by synthetic receptor cyclodextrin: effect of fluorescence modification of the protein and cavity size of the receptor in the interaction. *J. Mol. Recognit.* 26(11), 568–577 (2013).

25 Lebel CP, Ischiropoulos H, Bondy SC. Evaluation of the probe 2',7'-dichlorofluorescin as an indicator of reactive oxygen species formation and oxidative stress. *Chem. Res. Toxicol.* 5(2), 227–231 (1992).

26 Cathcart R, Schwiers E, Ames BN. Detection of picomole levels of hydroperoxides using a fluorescent dichlorofluorescein assay. *Anal. Biochem.* 134(1), 111–116 (1983).

27 Sardar S, Chaudhuri S, Kar P, Sarkar S, Lemmens P, Pal SK. Direct observation of key photoinduced dynamics in a potential nano-delivery vehicle of cancer drugs. *Phys. Chem. Chem. Phys.* 17(1), 166–177 (2015).

28 Oecd. Test no. 423: acute oral toxicity – acute toxic class method. OECD Publishing. www.oecd-ilibrary.org

29 Basu S. Carbon tetrachloride-induced lipid peroxidation: eicosanoid formation and their regulation by antioxidant nutrients. *Toxicology* 189(1–2), 113–127 (2003).

30 Kabir N, Ali H, Ateeq M, Bertino MF, Shah MR, Franzel L. Silymarin coated gold nanoparticles ameliorates CCl_4-induced hepatic injury and cirrhosis through down regulation of hepatic stellate cells and attenuation of Kupffer cells. *R. Soc. Chem. Adv.* 4(18), 9012–9020 (2014).

31 Weber LWD, Boll M, Stampfl A. Hepatotoxicity and mechanism of action of haloalkanes: carbon tetrachloride as a toxicological model. *Crit. Rev. Toxicol.* 33(2), 105–136 (2003).

• **Describes the mechanism of carbon tetrachloride-induced hepatotoxicity.**

32 Johnston DE, Kroening C. Mechanism of early carbon tetrachloride toxicity in cultured rat hepatocytes. *Pharmacol. Toxicol.* 83(6), 231–239 (1998).

33 Rechnagel RO, Glende EA Jr. Carbon tetrachloride hepatotoxicity: an example of lethal cleavage. *CRC Crit. Rev. Toxicol.* 2(3), 263–297 (1973).

34 Muriel P. Regulation of nitric oxide synthesis in the liver. *J. Appl. Toxicol.* 20(3), 189–195 (2000).

35 Jaeschke H, Gores GJ, Cederbaum AI, Hinson JA, Pessayre D, Lemasters JJ. Mechanisms of Hepatotoxicity. *Toxicol. Sci.* 65(2), 166–176 (2002).

36 Hurkadale PJ, Shelar PA, Palled SG, Mandavkar YD, Khedkar AS. Hepatoprotective activity of amorphophallus paeoniifolius tubers against paracetamol-induced liver damage in rats. *Asian Pac. J. Trop. Biomed.* 2(1, Suppl.), S238–S242 (2012).

37 Vuda M, D'souza R, Upadhya S *et al.* Hepatoprotective and antioxidant activity of aqueous extract of Hybanthus enneaspermus against CCl_4-induced liver injury in rats. *Exp. Toxicol. Pathol.* 64(7–8), 855–859 (2012).

38 GraphPad. www.graphpad.com

39 Khan SN, Islam B, Yennamalli R, Sultan A, Subbarao N, Khan AU. Interaction of mitoxantrone with human serum albumin: Spectroscopic and molecular modeling studies. *Eur. J. Pharm. Sci.* 35(5), 371–382 (2008).

40 Mitra RK, Verma PK, Wulferding D *et al.* A molecular magnet confined in the nanocage of a globular protein. *Chemphyschem* 11(2), 389–393 (2010).

41 Wolf P. Biochemical diagnosis of liver disease. *Ind. J. Clin. Biochem.* 14(1), 59–90 (1999).

• **Describes the diagnostics tests used in clinical biochemistry for assesment of liver damage and hyperbilirubinemia.**

42 Wang M-Y, Anderson G, Nowicki D, Jensen J. Hepatic protection by noni fruit juice against CCl_4-induced chronic liver damage in female SD rats. *Plant Food Hum. Nutr.* 63(3), 141–145 (2008).

43 Janbaz KH, Saeed SA, Gilani AH. Protective effect of rutin on paracetamol- and CCl_4-induced hepatotoxicity in rodents. *Fitoterapia* 73(7–8), 557–563 (2002).

44 Paquet KJ, Kamphausen U. The carbon-tetrachloride-hepatotoxicity as a model of liver damage. First report: long-time biochemical changes. *Acta Hepato. Gastroenterol.* 22(2), 84–88 (1975).

45 Rajkapoor B, Jayakar B, Kavimani S, Murugesh N. Effect of dried fruits of carica papaya LINN on hepatotoxicity. *Biol. Pharm. Bull.* 25(12), 1645–1646 (2002).

46 Drotman RB, Lawhorn GT. Serum enzymes as indicators of chemically induced liver damage. *Drug Chem. Toxicol.* 1(2), 163–171 (1978).

47 Zalatnai A, Sarosi I, Rot A, Lapis K. Inhibitory and promoting effects of carbon tetrachloride-induced liver cirrhosis on the diethylnitrosamine hepatocarcinogenesis in rats. *Cancer Lett.* 57(1), 67–73 (1991).

48 Burr AW, Carpenter MR, Hines JE, Gullick WJ, Burt AD. Intrahepatic distribution of transforming growth factor-alpha (TGF alpha) during liver regeneration following carbon tetrachloride-induced necrosis. *J. Pathol.* 170(1), 95–100 (1993).

49 Naziroglu M, Cay M, Ustundag B, Aksakal M, Yekeler H. Protective effects of vitamin E on carbon tetrachloride-induced liver damage in rats. *Cell Biochem. Funct.* 17(4), 253–259 (1999).

50 Al-Shabanah OA, Alam K, Nagi MN, Al-Rikabi AC, Al-Bekairi AM. Protective effect of aminoguanidine, a nitric oxide synthase inhibitor, against carbon tetrachloride induced hepatotoxicity in mice. *Life Sci.* 66(3), 265–270 (2000).

51 Ogata I, Auster AS, Matsui A *et al.* Up-regulation of type I procollagen C-proteinase enhancer protein messenger RNA in rats with CCl_4-induced liver fibrosis. *Hepatology* 26(3), 611–617 (1997).

52 Mackinnon M, Clayton C, Plummer J *et al.* Iron overload facilitates hepatic fibrosis in the rat alcohol/low-dose carbon tetrachloride model. *Hepatology* 21(4), 1083–1088 (1995).

53 Natsume M, Tsuji H, Harada A *et al.* Attenuated liver fibrosis and depressed serum albumin levels in carbon tetrachloride-treated IL-6-deficient mice. *J. Leukoc. Biol.* 66(4), 601–608 (1999).

54 Theocharis SE, Margeli AP, Skaltsas SD, Spiliopoulou CA, Koutselinis AS. Induction of metallothionein in the liver of carbon tetrachloride intoxicated rats: an immunohistochemical study. *Toxicology* 161(1–2), 129–138 (2001).